Inorganic Chemistry

Article

pubs.acs.org/IC

Synthesis, Structure, and Properties of $Ln_2Ru_3Al_{15}$ (Ln = Ce, Gd): Comparison with $LnRu_2Al_{10}$ and $CeRu_4(Al,Si)_{15.58}$

Gregory Morrison,[†] Neel Haldolaarachchige,[‡] Chih-Wei Chen,[§] David P. Young,[‡] Emilia Morosan,[§] and Julia Y. Chan*[,†]

[†]Department of Chemistry [‡]Department of Physics and Astronomy Louisiana State University, Baton Rouge, Louisiana 70803-1804, United States

[§]Department of Physics and Astronomy, Rice University, Houston, Texas 77005, United States

Supporting Information

ABSTRACT: $Ln_2Ru_3Al_{15}$ (Ln = Ce, Gd) have been synthesized, and the competition between the growth of $Ce_2Ru_3Al_{15}$ and $CeRu_2Al_{10}$ has been studied. The structure of $Ce_2Ru_3Al_{15}$ was modified from the previously reported $Ce_2Ru_3Al_{15}$ structure, and the structure of $Gd_2Ru_3Al_{15}$ was determined for the first time. The magnetic and transport properties of $Ln_2Ru_3Al_{15}$ were measured and compared to the properties of $LnRu_2Al_{10}$. $Gd_2Ru_3Al_{15}$ orders antiferromagnetically at 21.0 K with a spin reorientation at 4.1 K and has a positive paramagnetic Curie–Weiss temperature of 11.5(17) K, suggesting strong ferromagnetic interactions within the structure. $Ce_2Ru_3Al_{15}$ displays two low-temperature magnetic transitions at 3.7 and 3.1 K, the first of which is believed to be an antiferromagnetic ordering, with a θ_N of −7(3) K and a reduced moment of 2.33(4) μ_B/mol-Ce. Furthermore, the low-temperature magnetic and transport properties display the effects of Kondo screening of the magnetic moments. While structurally related, the properties of $Ce_2Ru_3Al_{15}$ do not display the same anomalous features observed in $CeRu_2Al_{10}$.

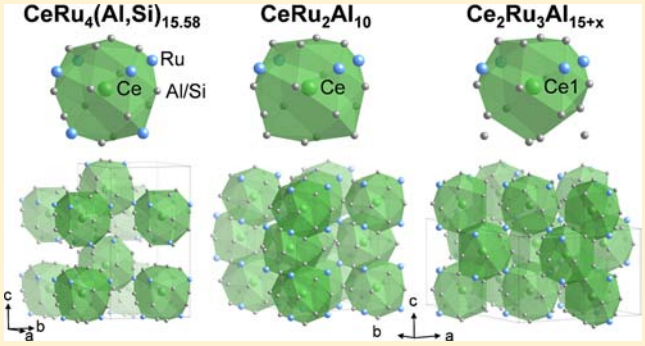

INTRODUCTION

$CeRu_2Al_{10}$, a member of the $YbFe_2Al_{10}$ structure type,[1] has received attention because it exhibits a metal-to-insulator transition and orders at 27 K,[2] higher than the 16 K antiferromagnetic (AFM) ordering of $GdRu_2Al_{10}$.[3] Single-crystal neutron scattering data indicates that the magnetic ordering is AFM with a (1,0,0) propagation vector[4] and a reduced moment of 0.34(2) μ_B/Ce at 1.5 K.[5] Furthermore, magnetic susceptibility displays a large degree of anisotropy. Both the anisotropy and the reduced moment can be attributed to crystal electric field splitting,[6] where the first two splitting terms have been calculated to be 500 and 760 K.[7] While the AFM ordering has been well characterized, its origin remains in question. Two possible explanations for the ordering are a charge density wave formation[8] or a Spin-Peierls transition.[9] Recently, a computational study[10] on $CeRu_2Al_{10}$ suggested that the atoms in the Ce polyhedra are shifted from the lowest energy state structure by about 0.025 Å. Magnetic calculations on the computationally relaxed structure found it to have a nonmagnetic ground state, while calculations on the actual structure resulted in a competition between nonmagnetic and AFM states. This suggests that the Ce polyhedra are important to the low-temperature properties of $CeRu_2Al_{10}$.[10]

In an effort to explore the relationship between the structure and the properties of $CeRu_2Al_{10}$, we studied the effect of the rare earth on the properties of $LnRu_2Al_{10}$ (Ln = lanthanide).[11] $PrRu_2Al_{10}$ displays paramagnetic behavior down to 13.2 K, when it enters a nonmagnetic singlet ground state due to crystal electric field splitting of the f orbitals, and has a large paramagnetic Curie–Weiss temperature of −49.8(14) K. $GdRu_2Al_{10}$ was found to order antiferromagnetically at 15.5 K with θ_N = −15.45(8) K. $YbRu_2Al_{10}$ is a Pauli paramagnet, indicating that Yb is in its divalent state. All three analogues display metallic behavior, although $GdRu_2Al_{10}$ is a poor metal with a resistivity on the order of 1 mΩ·cm.[11]

In order to further explore the role of the structure of $CeRu_2Al_{10}$ on the properties we have grown $CeRu_4(Al,Si)_{15.58}$, a member of the $NdRh_4Al_{15.37}$ structure type,[12] which contains Ce polyhedra that closely resemble the Ce environment in $CeRu_2Al_{10}$. However, instead of the face-sharing columns seen in $CeRu_2Al_{10}$, polyhedra in $CeRu_4(Al,Si)_{15.58}$ form corner-sharing sheets. $CeRu_4(Al,Si)_{15.58}$ follows a Curie–Weiss law with θ = −21.9(14) K but does not order down to 3 K. The resistivity displays a negative temperature dependence but does not follow the activated behavior ($\rho = \rho_o e^{-EG/2kT}$) typical of semiconductors.[13]

Another structure type which is related to $YbFe_2Al_{10}$ is the $Ce_2Ru_3Al_{15}$ structure type.[14] Like $CeRu_4(Al,Si)_{15.58}$, $Ce_2Ru_3Al_{15}$ contains Ce polyhedra which are similar to those in $CeRu_2Al_{10}$.

Received: December 7, 2012
Published: February 25, 2013

   dx.doi.org/10.1021/ic302693n | Inorg. Chem. 2013, 52, 3198–3206

Furthermore, these polyhedra form face-sharing columns much like the columns in $CeRu_2Al_{10}$. It is therefore of interest to study the properties of $Ce_2Ru_3Al_{15}$ in order to gain a better understanding of how both the Ce environment *and* the packing of the Ce polyhedra influence the properties. Herein, we report on the synthesis, structure, and properties of $Ln_2Ru_3Al_{15}$ (Ln = Ce, Gd) and compare them to the properties of $LnRu_2Al_{10}$.

EXPERIMENTAL SECTION

Synthesis. Three synthesis methods were utilized in an attempt to grow phase-pure $Ce_2Ru_3Al_{15}$. The first technique, flux growth, uses a low-melting metal as a solvent, or flux, in order to dissolve metals with higher melting points. The reactant metals are heated in a high-temperature muffle furnace which allows for fine-tuned temperature control and often results in growth of single crystals. However, in order to prevent the reactant metals from oxidizing, the reactions are typically sealed in an evacuated fused silica tube. As fused silica begins to become molten at ∼1250 °C, the maximum temperature available to flux growth is about 1200 °C. A second technique, radiofrequency (RF) induction heating, applies an alternating current to a coil, creating an alternating magnetic field. An alumina crucible wrapped with tantalum foil is placed in an argon environment in the center of the coil. The magnetic field creates eddy currents in the tantalum foil, which leads to resistive heating of the foil and, in turn, heats the crucible. Because the sample is in an inert environment, higher temperatures can be reached than in the flux method. Furthermore, by changing the applied current or partially raising the sample out of the coil, the temperature can be controlled. However, because an alumina crucible is used, the maximum temperature is limited by the melting point of alumina, 2053 °C.[15] A third technique, arc melting, uses an arc of electricity in order to melt the reactant metals under an argon atmosphere. This technique heats the reaction to ∼3000−4000 °C. However, arc melting provides little temperature control, and the rapid heating and cooling involved results in a polycrystalline sample.

Ce (Pieces, 99.9% metal basis excluding Ta), Gd (Pieces, 99.9% metal basis excluding Ta), Al (Shot, 99.999%), and Ru (Powder, 99.9%) were used as received. For flux growth reactions, the elements were loaded into an alumina crucible, covered with a second crucible, and sealed in an evacuated fused silica tube. Individual reaction ratios and temperature profiles for growth will be discussed in the Results and Discussion section. After the heating cycles were complete, reactions were inverted and centrifuged to remove any excess flux. For radiofrequency induction furnace growths, the reactant metals were loaded into an alumina crucible which was wrapped in tantalum foil. The crucible was placed in the furnace chamber, which was evacuated and flushed with Ar three times and then pressurized with Ar during heating. Temperature was increased (∼100 °C/min) until the sample was completely melted. Sample was further heated and dwelled for ∼10 min before being quick cooled (∼100 °C/min) to room temperature. Unfortunately, the utilized induction furnace is not equipped with a temperature probe. However, based on previous experience with the furnace and experimental results (vide infra) it is believed that the reaction temperature was above the 1200 °C maximum achieved by the conventional flux method. For growths via arc melting, reactant metals were placed on a copper hearth in the arc furnace chamber. The chamber was evacuated and flushed with Ar three times and then pressurized with Ar. The reactant metals were melted into a button which was turned over and remelted three times to ensure homogeneity. In order to minimize mass loss, the ruthenium powder was initially arc melted into buttons before being used for synthesis of $Ln_2Ru_3Al_{15}$. Mass loss in these reactions ranged from 0.53% to 1.16%. Arc-melted samples were placed in alumina crucibles and sealed in quartz tubes filled with a partial pressure of argon prior to annealing. A partial pressure was used such that the internal pressure and external pressure were similar in order to help maintain tube integrity during long, high-temperature dwells.

Structure. Structure determination was performed using single-crystal X-ray diffraction data. For $Ce_2Ru_3Al_{15}$, a single crystal was obtained from an aluminum-poor flux growth reaction, and for $Gd_2Ru_3Al_{15}$, a single crystal was extracted from an arc-melted pellet. Data collection was performed using an Enraf Nonius KappaCCD diffractometer with a Mo Kα source (λ = 0.71073 Å). Direct methods using SIR97[16] were performed in order to obtain an initial structural model which was then refined using SHELXL-97.[17] Crystallographic data and atomic positions for $Ln_2Ru_3Al_{15}$ can be found in Tables 1 and 2, respectively. In order to determine reaction products and ensure that the annealed arc-melted buttons were phase pure, powder X-ray diffraction was performed using a Bruker AXS D8 Advance Diffractometer with a Cu Kα source (λ = 1.54056 Å) equipped with a Ge incident beam monochromator. Data were collected for 5° ≤ 2θ ≤ 80°.

Table 1. Crystallographic Data for $Ln_2Ru_3Al_{15}$ (Ln = Ce, Gd)

formula	$Ce_2Ru_3Al_{15.04}$	$Gd_2Ru_{3.08}Al_{15}$
space group	$P6_3/mcm$	$P6_3/mcm$
a (Å)	13.1210(10)	13.0320(10)
c (Å)	9.0970(10)	9.0590(10)
V (Å^3)	1356.3(2)	1332.4(2)
Z	4	4
cryst dimens (mm^3)	0.13 × 0.15 × 0.15	0.03 × 0.03 × 0.13
temp. (K)	295(1)	295(1)
density (g cm^{-3})	4.845	5.137
θ range (deg)	1.79−30.99	1.80−30.98
μ (mm^{-1})	10.784	14.184
data collection and refinement		
no. of collected reflns	5182	4760
no. of unique reflns	813	799
R_{int}	0.0256	0.0309
h	$-19 \le h \le 19$	$-18 \le h \le 18$
k	$-15 \le k \le 15$	$-15 \le k \le 15$
l	$-13 \le l \le 12$	$-12 \le l \le 13$
$\Delta\rho_{max}$ (e Å^{-3})	1.409	1.803
$\Delta\rho_{min}$ (e Å^{-3})	−0.882	−2.134
GoF	1.181	1.091
extinction coefficient	0.00325(9)	0.00091(8)
$R_1(F)$ for $F_o^2 > 2\sigma(F_o^2)^a$	0.0192	0.0218
$R_w(F_o^2)^b$	0.0390	0.0527

$^aR_1 = \Sigma||F_o| - |F_c||/\Sigma|F_o|$. $^bwR_2 = [\Sigma w(F_o^2 - F_c^2)^2/\Sigma w(F_o^2)^2]^{1/2}$; $P = (F_o^2 + 2F_c^2)/3$; $w = 1/[\sigma^2(F_o^2) + (0.0129P)^2 + 3.6920P]$ and $w = 1/[\sigma^2(F_o^2) + (0.0247P)^2 + 6.3560P]$ for Ce and Gd analogues, respectively.

Energy-dispersive X-ray spectroscopy was performed on a single crystal of $Ce_2Ru_3Al_{15}$ from an aluminum-poor flux growth using a FEI Quanta 200 SEM equipped with an EDAX detector. Data were collected for six different locations on a single crystal, and the average and standard deviation were taken as the composition and uncertainty, respectively. The determined composition of the sample, normalized to Ce, was $Ce_{2.0(3)}Ru_{2.59(16)}Al_{13.4(5)}$.

Physical Properties. Physical properties were measured on polycrystalline annealed arc-melted samples of $Ln_2Ru_3Al_{15}$ which were sanded into bar shapes. Magnetic and electrical transport properties were measured using a Quantum Design Physical Property Measurement System (QD PPMS). Zero-field-cooled dc magnetic susceptibility was measured as a function of temperature from 3 to 290 K, and field-dependent magnetization was measured up to an applied field of 9 T. Resistivity was measured from 3 to 290 K, and magnetoresistance was measured from 0 to 9 T at 3 K using the standard four-probe method with an excitation current of 5.13 mA. H = 0 heat capacity was measured in a QD PPMS using an adiabatic relaxation technique for temperatures between 2 and 50 K.

dx.doi.org/10.1021/ic302693n | Inorg. Chem. 2013, 52, 3198−3206

Table 2. Atomic Coordinates and Atomic Displacement Parameters for $Ln_2Ru_3Al_{15}$ (Ln = Ce, Gd)

atom	Wyckoff site	x	y	z	U_{eq} (Å^2)[a]	occ.
$Ce_2Ru_3Al_{15.04}$						
Ce(1)	6*g*	0.60512(2)	0	1/4	0.00674(8)	1
Ce(2)	2*a*	0	0	1/4	0.00551(15)	0.825(2)
Ce(3)	4*e*	0	0	0.2219(6)	0.00551(15)	0.0874(12)
Ru(1)	12*i*	0.203474(11)	0.40695(2)	0	0.00532(8)	1
Al(1)	12*k*	0.79755(8)	0	0.02717(13)	0.0082(2)	1
Al(2)	12*i*	0.40892(5)	0.81785(10)	0	0.0078(2)	1
Al(3)	12*j*	0.16673(10)	0.87969(9)	1/4	0.0075(2)	1
Al(4)	12*j*	0.72320(10)	0.47613(9)	1/4	0.0087(2)	1
Al(5)	12*k*	0.61777(8)	0	0.89713(13)	0.0077(2)	1
Al(6)	2*b*	0	0	0	0.004(5)	0.0874(12)
$Gd_2Ru_{3.08}Al_{15}$						
Gd(1)	6*g*	0.60675(2)	0	1/4	0.00804(10)	1
Gd(2)	2*a*	0	0	1/4	0.00738(17)	0.670(2)
Gd(3)	4*e*	0	0	0.2093(4)	0.00738(17)	0.1649(11)
Ru(1)	12*i*	0.203187(14)	0.40637(3)	0	0.00588(11)	1
Ru(2)	2*b*	0	0	0	0.0196(13)	0.1649(11)
Al(1)	12*k*	0.79815(10)	0	0.02826(17)	0.0094(3)	1
Al(2)	12*i*	0.40949(6)	0.81898(12)	0	0.0085(3)	1
Al(3)	12*j*	0.16530(13)	0.87973(12)	1/4	0.0084(3)	1
Al(4)	12*j*	0.72567(13)	0.47679(12)	1/4	0.0097(3)	1
Al(5)	12*k*	0.61650(10)	0	0.89787(17)	0.0084(3)	1

[a] U_{eq} is defined as one-third of the trace of the orthogonalized U_{ij} tensor.

RESULTS AND DISCUSSION

Synthesis. Initially, growth of $Ce_2Ru_3Al_{15}$ was attempted using the self-flux method. However, its synthesis proved difficult due to the stability of $CeRu_2Al_{10}$. A graphical depiction of the competition between the two phases is shown in Figure 1. When an excess of flux is used, the reaction favors growth of $CeRu_2Al_{10}$. Dwelling a reaction with a Ce:Ru:Al ratio of 2:3:18 at 1200 °C for 24 h before cooling to 720 °C at 5 °C/h only yielded $CeRu_2Al_{10}$. When stoichiometric amounts of the reactant metals were used, reaction products were found to be highly dependent on reaction temperature. When the reaction was dwelled at 1050 °C, polycrystalline $CeRu_2Al_{10}$ and Ru_4Al_{13} were grown with none of the desired $Ce_2Ru_3Al_{15}$. Raising the dwell temperature to 1200 °C yielded polycrystalline $Ce_2Ru_3Al_{15}$ as the majority product with large amounts of $CeRu_2Al_{10}$ and Ru_4Al_{13} as impurities. The results of higher temperature syntheses will be discussed in the next paragraph. Single-crystalline $Ce_2Ru_3Al_{15}$ can be grown using the self-flux method with flux poor reaction ratios. Reactions with Ce:Ru:Al ratios of either 2:3:12 or 3:4:12, which were dwelled at 1200 °C, sometimes yielded single-crystalline $Ce_2Ru_3Al_{15}$ imbedded in a matrix of binaries. However, crystals were too small and difficult to extract to be able to be used for measurement of physical properties.

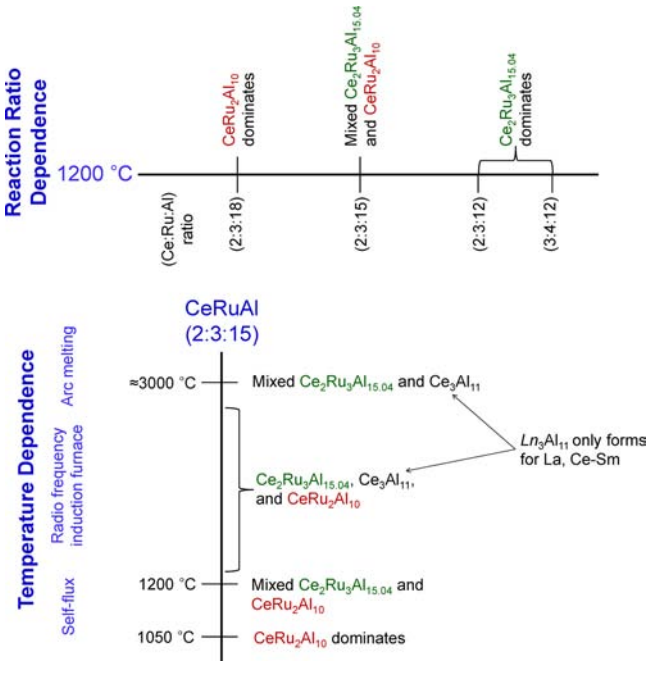

Figure 1. Two schematics showing the products of flux growth reactions dwelled at 1200 °C with various reactant ratios and products of reactions with a Ce:Ru:Al composition of 2:3:15 heated to various temperatures.

Following the failure to obtain large, extractable single crystals using the flux growth method, growth of $Ce_2Ru_3Al_{15}$ was attempted using higher temperature synthesis methods, as the former flux-grown stoichiometric reactions suggested that higher temperatures favored formation of $Ce_2Ru_3Al_{15}$ over $CeRu_2Al_{10}$ and Ru_4Al_{13}. $Ce_2Ru_3Al_{15}$ growth was attempted by arc melting on stoichiometry, and as expected, no $CeRu_2Al_{10}$ was present in the final button. However, the high temperatures stabilized a different impurity phase, Ce_3Al_{11}, which was present in the button along with $Ce_2Ru_3Al_{15}$. In an attempt to eliminate all three impurities, intermediate-temperature growth was performed on stoichiometry using an RF induction furnace. This growth was found to contain $Ce_2Ru_3Al_{15}$, $CeRu_2Al_{10}$, and Ce_3Al_{11}, indicating that there is no ideal temperature regime which avoids growth of all impurities.

Although no optimal temperature was found to grow $Ce_2Ru_3Al_{15}$ on stoichiometry, phase purity of the arc-melted pellet can be obtained by annealing. When annealing at low temperatures, ca. 800 °C, $CeRu_2Al_{10}$ forms in the sample. In

dx.doi.org/10.1021/ic302693n | Inorg. Chem. 2013, 52, 3198−3206

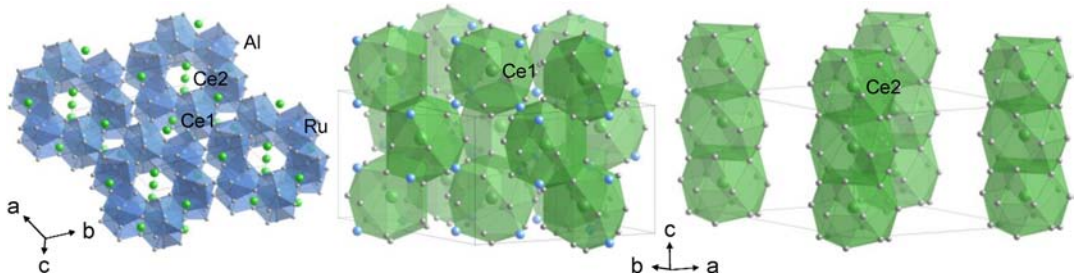

Figure 2. (a) Structure of $Ce_2Ru_3Al_{15}$ showing the Ru polyhedra, and (b) Ce(1) sublattice and (c) Ce(2) sublattice. Ce(3) and Al(6) sites are omitted for clarity.

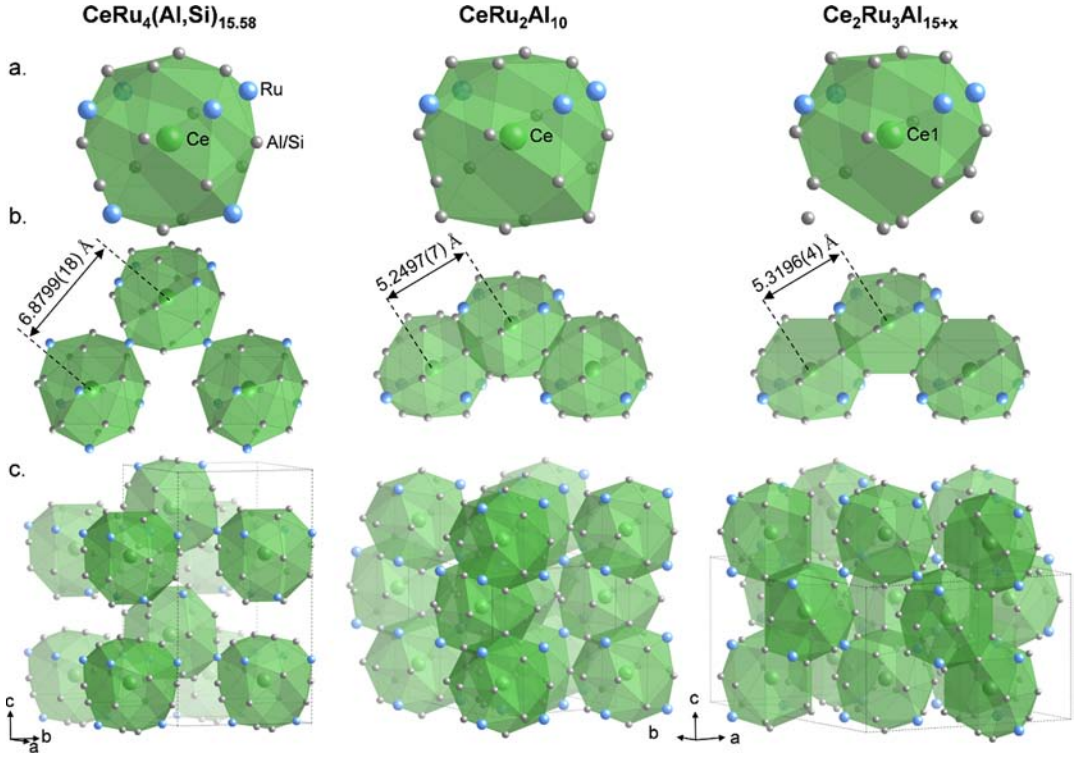

Figure 3. Comparison of Ce(1) environments in $CeRu_4(Al,Si)_{15.58}$, $CeRu_2Al_{10}$, and $Ce_2Ru_3Al_{15}$ showing the (a) Ce(1) polyhedra, (b) Ce(1)−Ce(1) nearest neighbors, and (c) packing of the Ce(1) polyhedra within the unit cells.

order to avoid this, annealing at 1150 °C is required. By annealing at this temperature for 6 days, almost-phase-pure $Ce_2Ru_3Al_{15}$ was obtained. In attempt to anneal out the remaining impurity (a small, unidentified impurity resulting in a diffraction peak at $2\theta = 73.8°$), a sample was annealed at 1150 °C for 12 days. However, this longer annealing time led to formation of $CeRu_2Al_{10}$. Thus, samples of phase-pure $Gd_2Ru_3Al_{15}$ and almost-phase-pure $La_2Ru_3Al_{15}$ were also prepared via arc melting and annealing for 6 days.

Structure. $Ce_2Ru_3Al_{15}$ crystallizes in the hexagonal space group $P6_3/mcm$ with $a = 13.1210(10)$ Å and $c = 9.0970(10)$ Å. $Gd_2Ru_3Al_{15}$ is reported for the first time and has lattice parameters $a = 13.0320(10)$ Å and $c = 9.0590(10)$ Å. This structure type has also been reported for $Ln_2Os_3Al_{15}$ (Ln = Nd, Sm, Gd) as an impurity product in arc-melted pellets of $LnOs_2Al_{10}$.[18] Initially, structural models of $Ln_2Ru_3Al_{15}$ were refined in agreement with the previously reported structure of $Ce_2Ru_3Al_{15}$.[14] In this model there is one Ru site and two lanthanide sites. Each Ru(1) atom is surrounded by 10 Al atoms, forming a distorted pentagonal antiprism which is bicapped by Ln(1) atoms such that the point symmetry is 2. Ru−Al distances, 2.5673(3)−2.6912(6) Å (Ce) and 2.5564(3)−2.6772(8) Å (Gd), are close to the sum of their covalent radii, while the two Ru−Ln(1) interactions, 3.4500(3) Å (Ce) and 3.4230(3) Å (Gd), are >0.5 Å outside of bonding. As shown in Figure 2a, each Ru(1) polyhedron is edge sharing with two other polyhedra and six of these polyhedra form a ring. Each polyhedron within the ring is also corner sharing with two other rings. This generates triangular and quadrilateral channels within the Ru−Al sheets. These sheets lie in the *ab* plane and are edge sharing in the *c* direction. The Ru sheets resemble the sheets seen in $Ru_{23}(Al,Si)_{97}$ of the α-AlFeSi structure type.[13]

The Ln1 polyhedra lie in the square channels created by the Ru sublattice. Each Ln(1) atom is surrounded by 14 Al and 4 Ru atoms with point symmetry *mm*. The Ln(1) polyhedra resemble the 20 coordinate Ln polyhedral seen in $LnRu_2Al_{10}$[1] and $CeRu_4(Al,Si)_{15.58}$.[13] Ln(1)−Al [3.1438(11)−3.3703(7) Å (Ce) and 3.1037(14)−3.3524 Å (Gd)] and Ln(1)−Ru distances [3.4500(3) Å (Ce) and 3.4230(3) Å (Gd)], while larger than the sums of the covalent radii, are similar to the distances seen in the respective analogues of the other two

dx.doi.org/10.1021/ic302693n | *Inorg. Chem.* 2013, 52, 3198−3206

structure types. As shown in Figure 2b, each Ln(1) polyhedron is face sharing with two other Ln(1) polyhedra to form columns in the *c* direction. These columns are edge sharing with each other through the Ru(1) atoms.

Figure 3a compares the Ce(1) environment in $Ce_2Ru_3Al_{15}$ to the Ce environments in $CeRu_2Al_{10}$ and $CeRu_4(Al,Si)_{15.58}$. As stated above, the 18-coordinate Ce(1) polyhedra in $Ce_2Ru_3Al_{15}$ are closely related to the 20-coordinate Ce polyhedra in the other two compounds. The main difference between these three polyhedra concerns two equivalent atoms. In $CeRu_4(Al,Si)_{15.58}$ these two atoms are Ru2 atoms, and the Ce−Ru2 distances are comparable to the other Ce−Ru distances in the polyhedra. In $CeRu_2Al_{10}$, these atoms are Al(1) atoms and the Ce−Al(1) distances are approximately 0.36 Å larger than the other Ce−Al distances. In $Ce_2Ru_3Al_{15}$, these atoms are Al8 atoms but the Ce1−Al8 distances are over 0.5 Å larger than the largest Ce(1)−Al distance, and therefore, the Al8 atoms are no longer considered part of the Ce(1) polyhedron. Figure 3b shows the packing of the Ce(1) polyhedra in each compound. The Ce polyhedra in $Ce_2Ru_3Al_{15}$ and $CeRu_2Al_{10}$ pack in the same way, that is, they form face-sharing columns in the *c* direction. While packing in the same way, the Ce(1)−Ce(1) distances in $CeRu_2Al_{10}$, 5.2497(7) Å, are somewhat closer than in $Ce_2Ru_3Al_{15}$, 5.3196(4) Å. The Ce polyhedra in $CeRu_4(Al,Si)_{15.58}$, on the other hand, form corner-sharing columns in the *b* direction through the Ru(2) atoms. Due to the fact that they are corner sharing, the Ce(1)−Ce(1) distances in $CeRu_4(Al,Si)_{15.58}$ of 6.8799(18) Å are considerably larger than in the other two compounds.[13] It is important to note that while Ce(1) is the only Ce site in $CeRu_2Al_{10}$ and $CeRu_4(Al,Si)_{15.58}$, this is not the case in $Ce_2Ru_3Al_{15}$. A comparison of all of the Ln−Ln contact distances in each structure can be found in Table 3 and will be discussed later.

Table 3. Comparison of Ln−Ln Distances between Titled Structure Types

interaction	Ce (Å)	Gd (Å)	ref
$LnRu_4(Al,Si)_{15.58}$			
Ln(1)−Ln(1)	6.8799(18)		13
$LnRu_2Al_{10}$			
Ln(1)−Ln(1)	5.2497(7)	5.2516(7)	11
$Ln_2Ru_3Al_{15}$			
Ln(1)−Ln(1)	5.3196(4)	5.3158(5)	
Ln(1)−Ln(2)	5.1812(3)	5.1248(4)	
Ln(1)−Ln(3)	5.1875(4)	5.1381(5)	
Ln(2)−Ln(2)	4.5485(5)	4.5295(5)	
Ln(2)−Ln(3)	4.293(6)	4.161(4)	
Ln(3)−Ln(3)	5.060(8)	5.267(5)	

While the Ce(1) columns in $CeRu_2Al_{10}$ and $Ce_2Ru_3Al_{15}$ are similar, they pack in different ways, as can be seen in Figure 3c. In both compounds the columns are corner sharing through the Ru atoms, but in $CeRu_2Al_{10}$ the columns are aligned with each other, while in $Ce_2Ru_3Al_{15}$ each column is rotated 120° with respect to the adjacent columns.

The Ln2 polyhedra lie in the center of the six-membered Ru polyhedral rings. Each Ln(2) is surrounded by 18 Al atoms with point symmetry −6*m*2. The Ln(2)−Al distances range from 3.2759(11) to 3.6625(9) Å (Ce) and 3.2363(14) to 3.6433(12) Å (Gd). The Ln(2) polyhedra form volume-sharing columns in the *c* direction, as shown in Figure 2c. Each Ln(2) polyhedron is also face sharing with three Ln(1) polyhedra in the *ab* plane.

Following the initial refinement of the models using the previously reported structure of $Ce_2Ru_3Al_{15}$, the largest residual electron density was 3.931 and 18.869 $e^-/Å^3$ for the Ce and Gd analogues, respectively. These Q peaks were located at the origin with the closest contacts being two Ln(2) atoms 2.27 (Ce) or 2.26 (Gd) Å away. Because of the close proximity of the Ln(2) contacts, it was believed that the site was a partially occupied Al or Ru atom. Due to the partial occupancy of the site, either atom resulted in the same quality structural model. For the Ce analogue the resulting site occupancies were 8.5(13)% (Al) and 2.4(4)% (Ru), and for the Gd analogue the occupancies were 46.5(16)% (Al) and 13.5(4)% (Ru). While the identity of the atom cannot be determined by looking at the site, it can be determined from the splitting of the Ln(2) site. Since the Ln(2) contacts are inside the sum of the covalent radii, when the partially occupied atom is present, the adjacent Ln(2) atoms are pushed off the mirror plane to a Ln(3) site. Because of the closeness of the Ln(2) and Ln(3) sites, the atomic displacement parameters of these sites had to be refined isotropically. The occupancy of the Ln(3) site was found to be 9.0(14)% for the Ce analogue and 17.8(4)% for the Gd analogue. Comparing these occupancies to the Al or Ru occupancies reveals that the partially occupied site is an Al site [Al(6)] for the Ce analogue and a Ru site [Ru(2)] for the Gd analogue. Since the occupancy of Ln(3) should equal that of Al(6) or Ru(2), the occupancies of the sites were then confined. This resulted in an Al(6) occupancy of 8.72(12)% and a Ru(2) occupancy of 16.49(11)%. On the basis of these occupancies, the resulting stoichiometries are $Ce_2Ru_3Al_{15.04}$ and $Gd_2Ru_{3.08}Al_{15}$. For simplicity, the two analogues will continue to be referred to using the $Ln_2Ru_3Al_{15}$ stoichiometry.

The Ln(3) site is surrounded by 15 Al atoms and either an Al(6) or a Ru(2) atom with point symmetry 3. Ln(3)−Al distances range from 3.193(3) to 3.502(4) Å (Ce) and 3.100(2) to 3.546(3) Å (Gd). The Ce(3)−Al(6) contact is 2.530(5) Å, and the Gd(3)−Ru(2) contact is 2.663(3) Å, both of which are closer than the sum of their covalent radii, 2.90 and 2.85 Å, respectively.[19] The closer Ce−Al contact, despite the larger sum of covalent radii, suggests that Ce(3) is tetravalent. The different atom types in the two structures does not appear to be a structural effect, as Ru and Al have very close covalent radii and similar interatomic distances within Ln−Ru−Al compounds.[11,20,21] On the other hand, the structural difference may be an electronic effect. Tetravalent Ce donates more electrons to the conduction band than Gd^{3+}. This difference is counteracted by the fact that Ru has a greater number of valence electrons than does Al.

Excluding the disordered Ln(3), the closest Ln−Ln contacts within $Ln_2Ru_3Al_{15}$ are between volume-sharing Ln(2) polyhedra and 4.5485(5) (Ce) and 4.5295(5) (Gd) Å. The Ln(1)−Ln(1) contacts are 5.3196(4) (Ce) and 5.3158(5) (Gd) Å, which is farther than the contacts found in $LnRu_2Al_{10}$ (5.2497(7) (Ce) and 5.2516(7) (Gd) Å). The Ln(1)−Ln(2) contacts, which are closer than the Ln(1)−Ln(1) contacts and the $LnRu_2Al_{10}$ contacts, are 5.1812(3) (Ce) and 5.1248(4) (Gd) Å. These distances along with the Ln−Ln(3) distances can be found in Table 4.

PHYSICAL PROPERTIES

Magnetization. Table 5 summarizes the magnetic data for $LnRu_2Al_{10}$ and $Ln_2Ru_3Al_{15}$ (Ln = Ce, Gd). Figure 4a shows the magnetic susceptibility of $Ce_2Ru_3Al_{15}$ as a function of temperature at an applied field of 0.1 T. The inset shows the

dx.doi.org/10.1021/ic302693n | Inorg. Chem. 2013, 52, 3198−3206

Table 4. Select Interatomic Distances in $Ln_2Ru_3Al_{15}$ (Ln = Ce, Gd) (Angstroms)

interaction	$Ce_2Ru_3Al_{15.04}$	$Gd_2Ru_{3.08}Al_{15}$
Ln(1)−Ru(1) (×4)	3.4500(3)	3.4230(3)
Ln(1)−Al(1) (×2)	3.2380(12)	3.2026(15)
Ln(1)−Al(2) (×4)	3.3703(7)	3.3524(9)
Ln(1)−Al(3) (×2)	3.1438(11)	3.1037(14)
Ln(1)−Al(4) (×2)	3.1477(12)	3.0976(15)
Ln(1)−Al(5) (×2)	3.2144(12)	3.1925(16)
Ln(1)−Al(5) (×2)	3.2162(11)	3.2029(14)
Ln(2)−Al(1) (×6)	3.3414(11)	3.3098(14)
Ln(2)−Al(1) (×6)	3.6625(9)	3.6433(12)
Ln(2)−Al(3) (×6)	3.2759(11)	3.2363(14)
Ln(3)−Al(1) (×3)	3.193(3)	3.100(2)
Ln(3)−Al(1) (×3)	3.491(4)	3.399(2)
Ln(3)−Al(1) (×3)	3.502(4)	3.546(3)
Ln(3)−Al(3) (×6)	3.2859(12)	2.2572(14)
Ln(3)−M[a] (×1)	2.530(5)	2.663(3)
Ru(1)−Ln(1) (×2)	3.4500(3)	3.4230(3)
Ru(1)−Al(1) (×2)	2.6879(6)	2.6690(8)
Ru(1)−Al(2) (×2)	2.5673(3)	2.5564(3)
Ru(1)−Al(3) (×2)	2.6686(6)	2.6597(7)
Ru(1)−Al(4) (×2)	2.6686(6)	2.6259(7)
Ru(1)−Al(5) (×2)	2.6912(6)	2.6772(8)
M[a]−Ln(3) (×2)	2.530(5)	2.633(3)
M[a]−Al(1) (×6)	2.6678(11)	2.6439(13)

[a]M = Al6 for Ce analogue and Ru2 for Gd analogue.

derivative of the susceptibility and highlights two apparent low-temperature transitions. Heat capacity data (vide infra) shows that these transitions are bulk transitions and occur at 3.7 and 3.1 K. Below 100 K, the inverse susceptibility drops below Curie−Weiss behavior, which can be attributed to crystalline electric field effects. Similar behavior has been observed in other rare earth intermetallics such as hexagonal CeNiIn[22] and orthorhombic $CePtSi_2$[23] and is expected as $CeRu_2Al_{10}$ was found to display considerable CEF effects.[7] Fitting from 100 to 290 K with a modified Curie−Weiss law $\chi = \chi_0 + C/(T - \theta)$, where χ_0 is a temperature-independent sum of the diamagnetic and Pauli paramagnetic contributions, yields a Curie−Weiss temperature of −7(3) K. The negative θ, coupled with the increase in $d\chi/dT$ below 3.7 K and the AFM ordering of $Gd_2Ru_3Al_{15}$, as shown below, suggests that the 3.7 K transition is an AFM ordering. An effective moment of 2.33(4) μ_B is determined from the Curie−Weiss fit at high temperatures and is less than the 2.54 μ_B expected for Ce^{3+}. Magnetization as a function of field, shown in Figure 4b, appears to saturate at ∼1.04 μ_B/Ce, which is smaller than the 2.14 μ_B expected for trivalent Ce.

The temperature-dependent magnetic susceptibility of $Gd_2Ru_3Al_{15}$ at 0.1 T, shown in Figure 5a, displays an AFM ordering at T_N = 21.0 K with a spin reorientation at 4.1 K, similar to the two spin reorientations observed in $Ce_2Ru_3Al_{15}$. Below 150 K, the inverse susceptibility deviates below Curie−Weiss behavior. This deviation is believed to be caused by a small FM impurity, below the detection limit of powder XRD, such as $GdAl_2$, which orders at ∼170 K, depending on sample purity and disorder.[24] Fitting with a modified Curie−Weiss law above 160 K yields an effective moment of 7.97(7) μ_B, close to the 7.94 μ_B expected for Gd^{3+}, and a θ of 11.5(17) K. This suggests that the Ru atoms are nonmagnetic. As the f orbital of Gd is half-filled, and therefore spherically symmetric, the positive Curie−Weiss temperature cannot be due to CEF effects. Therefore, a positive θ, despite the antiferromagnetic ordering, suggests strong ferromagnetic correlations within the structure. One possibility is that these correlations involve the Gd(3) atoms. As the Gd(2)−Gd(3) distance, 4.161(4) Å, is the closest distance in the structure, based on $1/r^3$ attenuation of the RKKY interaction,[25−27] a mechanism in which the conduction electrons mediate magnetic ordering, it may have the strongest J coupling. However, due to the partial occupancy of the Gd(3) site, no long-range order can exist. This would also explain the lack of a positive Curie−Weiss temperature in $Ce_2Ru_3Al_{15}$, as Ce(3) is believed to be tetravalent. Magnetization as a function of field is shown in Figure 5b and does not saturate up to 9 T. A broad transition, possibly a partial spin reorientation, is observed at $H \approx 2.5$ T.

Electrical Transport. Figure 6a and 6b shows the polycrystalline resistivity (a) and magnetoresistance (b) of $Ce_2Ru_3Al_{15}$ (green) and $Gd_2Ru_3Al_{15}$ (blue), respectively. Both analogues display a similar magnitude of resistivity, with $\rho_{290K} \approx$ 0.42 (Ce) and 0.55 mΩ·cm (Gd) and ρ_{2K} of 0.12 and 0.091 mΩ·cm (Gd). This leads to residual resistivity ratios, RRR = (ρ_{290K}/ρ_{2K}), of 3.4 (Ce) and 6.1 (Gd). These RRR values are smaller than the 8.9 observed for a single crystal of $GdRu_2Al_{10}$ and can be attributed to grain boundary scattering due to the polycrystalline nature of the samples. For $40 \leq T \leq 100$ K, the resistivity of $Gd_2Ru_3Al_{15}$ follows a T^2 dependence, shown in the inset of Figure 6a, which is typical of metallic compounds at low temperature.

Decreases in the resistivities at 5.3 (Ce) and 21.3 K (Gd) can be attributed to a loss of spin disorder scattering due to magnetic ordering. Prior to this decrease, the Ce analogue displays an upturn at 20 K, suggestive of the Kondo effect, a mechanism in which the conduction electrons screen the magnetic moment of the rare earths.[28] This is in agreement with the magnetoresistance (MR), which is negative for $Ce_2Ru_3Al_{15}$ and reaches −24% at 9 T. Before AFM ordering, the resistivity of $Gd_2Ru_3Al_{15}$ displays a small upturn at 26.3 K. Similar behavior was observed in $GdRu_2Al_{10}$[11] and may be due to formation of magnetic polarons prior to magnetic ordering, as observed in EuB_6.[29] The MR of $Gd_2Ru_3Al_{15}$ is positive, which is typical for intermetallics, and reaches 26% at 9 T. The magnitude of the MR is greater than in most intermetallic compounds. For example, $GdRu_2Al_{10}$, which orders antiferromagnetically at 15.5 K, with a spin reorientation at 7.8 K, has a MR of less than 1% at 9 T.[11] The large MR in $Gd_2Ru_3Al_{15}$ may be due to the proximity of the 3 K measurement temperature to

Table 5. Magnetic Properties for $LnRu_2Al_{10}$ and $Ln_2Ru_3Al_{15}$ (Ln = Ce, Gd)

	χ_o(emu/mol-Ln)	T_N (K)	θ (K)	μ_{calc} (μ_B)	μ_{eff} (μ_B)	fit range (K)	ref
$CeRu_2Al_{10}$		27.3	−44	2.54	3.03		32
$GdRu_2Al_{10}$	0.00015(4)	15.5	−15.45(8)	7.94	8.14(10)	50−275	11
$Ce_2Ru_3Al_{15}$	0.00018(7)	3.7	−7(3)	2.54	2.33(4)	100−290	
$Gd_2Ru_3Al_{15}$	0.0008(3)	21.0	11.5(17)	7.94	7.97(7)	160−288	

dx.doi.org/10.1021/ic302693n | Inorg. Chem. 2013, 52, 3198−3206

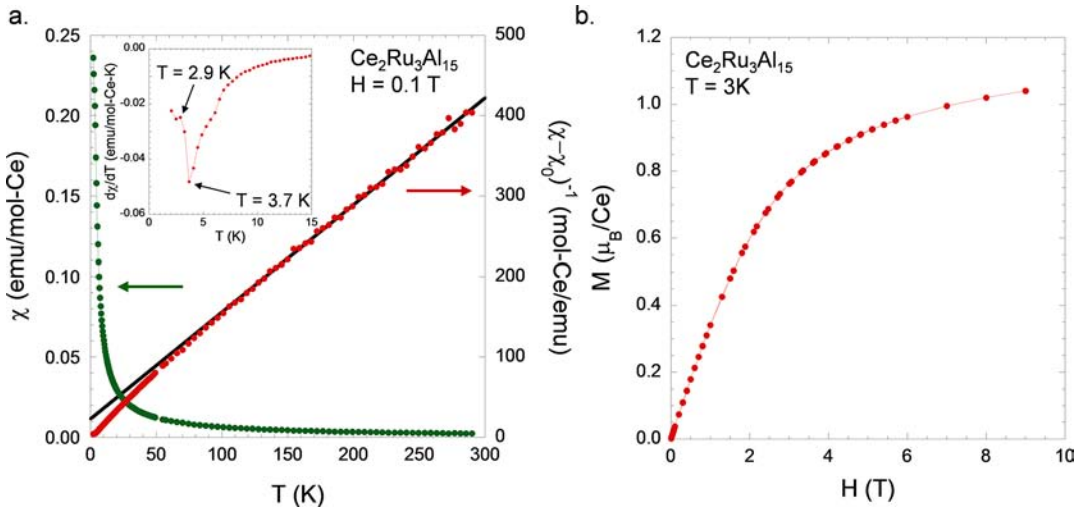

Figure 4. (a) Magnetic susceptibility and inverse susceptibility of $Ce_2Ru_3Al_{15}$. (Inset) Derivative of the susceptibility, highlighting two low-temperature transitions. (b) Field-dependent magnetization of $Ce_2Ru_3Al_{15}$.

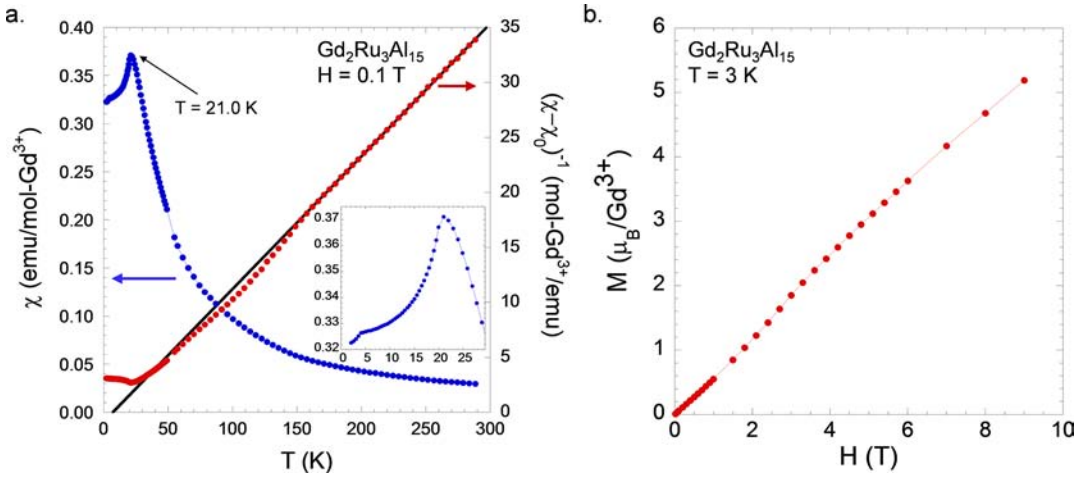

Figure 5. (a) Magnetic susceptibility and inverse susceptibility of $Gd_2Ru_3Al_{15}$. (Inset) Two low-temperature transitions. (b) Field-dependent magnetization of $Gd_2Ru_3Al_{15}$.

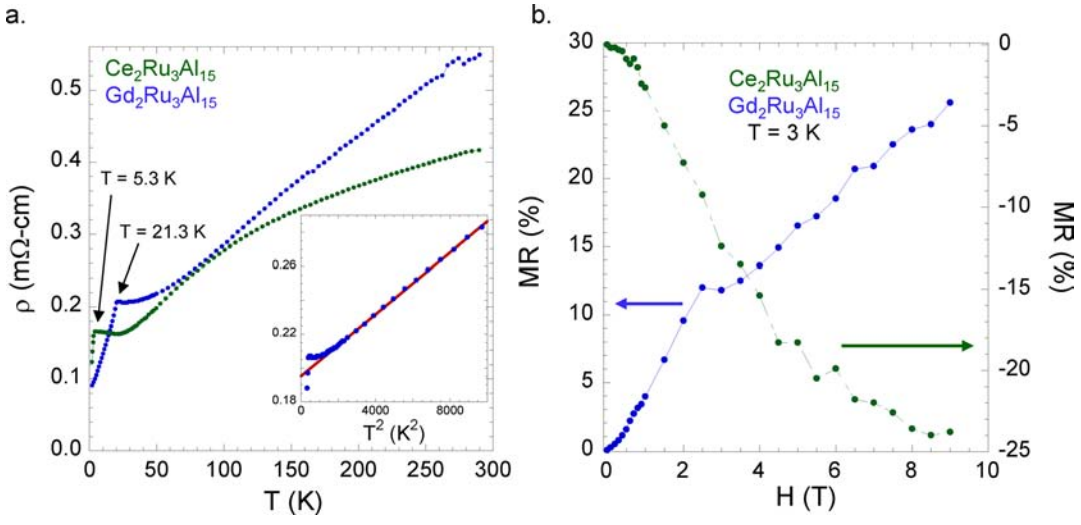

Figure 6. (a) Resistivity and (b) magnetoresistance of $Ln_2Ru_3Al_{15}$ (Ln = Ce, Gd). Inset in a highlights the low-temperature dependence of the resistivity for the Gd analogue.

dx.doi.org/10.1021/ic302693n | Inorg. Chem. 2013, 52, 3198−3206

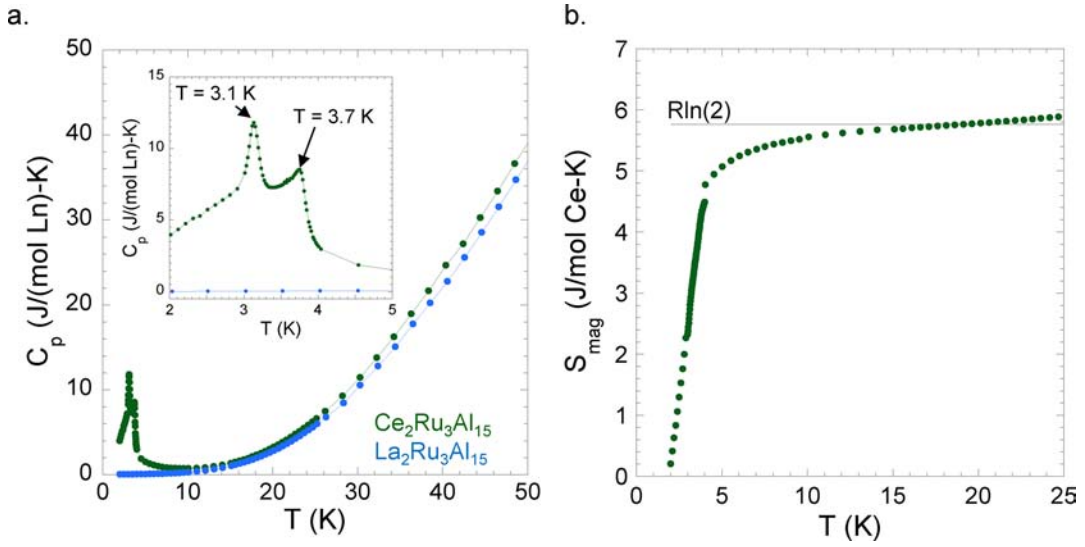

Figure 7. (a) Heat capacity of $Ln_2Ru_3Al_{15}$ (Ln = La, Ce). (Inset) Low-temperature transitions in the Ce analogue. (b) Magnetic entropy of $Ce_2Ru_3Al_{15}$ as a function of temperature. Solid line indicates Rln2.

the spin reorientation at 4.1 K. Enhanced MR has been observed in other intermetallics near magnetic transitions.[30,31] At 2.5 T, the MR changes slope, which can be attributed to the broad transition observed in the magnetization as a function of applied field.

Heat Capacity. Figure 7 shows the specific heat capacity of $Ln_2Ru_3Al_{15}$ (Ln = La, Ce). The low-temperature data, emphasized in the inset, displays two transitions in $Ce_2Ru_3Al_{15}$ at 3.7 and 3.1 K. Typically, the low-temperature heat capacity of metals follows $C_p = \gamma T + \beta T^3$, where γ is the electronic specific heat coefficient and βT^3 is the phonon contribution to the specific heat. The nonmagnetic contribution to the specific heat can be approximated as the specific heat of a nonmagnetic analogue and subtracted from C_p to obtain C_m, the magnetic specific heat. The specific heat of the La analogue was subtracted from the Ce analogue in order to obtain C_m. For a magnetic transition, $R\ln(2J + 1)$ of entropy (S_m) should accompany the transition, where J is the total angular momentum. Integrating the magnetic entropy of $Ce_2Ru_3Al_{15}$ from 2 to 15 K recovers $S_m \approx R\ln 2$ entropy, based on the trivalent Ce concentration from the susceptibility. The entropy is actually recovered prior to 15 K as the phase transition is still occurring below 2 K, and therefore, not all of the magnetic entropy has been integrated. Due to the nonlinearity of C_m/T vs T^2 above the magnetic orderings, believed to be caused by small impurities in the arc-melted samples, the Sommerfeld coefficient was not determined.

Comparison of Structure Types. $GdRu_2Al_{10}$ orders antiferromagnetically at 15.5 K, while $Gd_2Ru_3Al_{15}$ orders antiferromagnetically at 21.0 K. Two Gd−Gd interactions are similar in distance to the 5.2516(7) Å distance in $GdRu_2Al_{10}$: the Gd(1)−Gd(1) interaction, 5.3158(5) Å, and the Gd(1)−Gd(2) interaction, 5.1248(4) Å. However, it is not readily apparent between which Gd atoms the AFM ordering occurs. $Gd_2Ru_3Al_{15}$, despite being polycrystalline, also has a lower resistivity at the ordering temperature, ∼0.2 mΩ·cm, than does $GdRu_2Al_{10}$, ∼0.3 mΩ·cm. This suggests that $Gd_2Ru_3Al_{15}$ has a higher carrier concentration, which would lead to stronger RKKY interactions.

On the basis of the 16 K ordering of $GdRu_2Al_{10}$ and deGennes scaling, $CeRu_2Al_{10}$ is expected to order at 0.1 K.[3] Instead, $CeRu_2Al_{10}$ shows an enhanced ordering temperature of 27 K.[2] A similar trend is not observed in $Ln_2Ru_3Al_{15}$, where the Gd analogue orders at 21.0 K and the Ce analogue orders at 3.7 K. Furthermore, $Ce_2Ru_3Al_{15}$ displays metallic resistivity over the entire measured temperature range, 2−290 K, unlike $CeRu_2Al_{10}$ which displays a metal-to-insulator transition at 27 K indicative of a narrow gap opening at the Fermi surface.[2] While structurally related to $CeRu_2Al_{10}$, it is apparent that $Ce_2Ru_3Al_{15}$ does not display the same anomalous behavior. The contrast in properties despite both structures containing very similar columns of Ce polyhedra suggests that either the properties are dependent on the packing of the columns within the unit cell or, as suggested in the computation study discussed in the Introduction, the properties of $CeRu_2Al_{10}$ arise due to small changes in the Ce polyhedra. Due to the similar structure but contrasting properties, $Ce_2Ru_3Al_{15}$ offers potential for further comparison studies with $CeRu_2Al_{10}$.

■ CONCLUSIONS

Synthesis of $Ce_2Ru_3Al_{15}$ is difficult due to the stability of $CeRu_2Al_{10}$ at low temperatures and in flux-rich melts and the stability of Ce_3Al_{11} at high temperatures. $Ln_2Ru_3Al_{15}$ (Ln = La, Ce, Gd) were synthesized by arc melting and annealing at 1150 °C for 6 days. The crystal structure was modified from the originally reported structure[14] in order to account for a partially occupied atom at the origin (2*b*) and the resulting splitting of the Ln(2) site into a Ln(2) site and a Ln(3) site. On the basis of the occupancy of the Ln(3) site, the 2*b* site was determined to be an Al atom in the Ce analogue and a Ru analogue in the Gd analogue.

$Gd_2Ru_3Al_{15}$ was found to order antiferromagnetically at 21.0 K with a spin reorientation at 4.1 K. The Curie−Weiss temperature was found to be positive, indicating FM interactions within the structure, possibly involving the partially occupied Gd(3) atoms. $Ce_2Ru_3Al_{15}$ displays two spin reorientations, the first of which is believed to be an AFM ordering, at low temperatures, 3.7 and 3.1 K, made apparent by $d\chi/dT$ and heat capacity measurements. Below 100 K, the susceptibility deviates below the Curie−Weiss fit which is characteristic of lost moment due to Kondo screening. This is supported by an upturn in the resistivity at 20 K and a negative

dx.doi.org/10.1021/ic302693n | Inorg. Chem. 2013, 52, 3198−3206

magnetoresistance of −24% at 9 T. $Ce_2Ru_3Al_{15}$ does not display the enhanced ordering temperature or metal-to-insulator transition observed in $CeRu_2Al_{10}$ despite the two structures containing similar columns of Ce polyhedra. For this reason, further comparison studies between the two compounds is warranted and could help elucidate the cause of the anomalous properties observed in $CeRu_2Al_{10}$.

■ ASSOCIATED CONTENT

Supporting Information

Single crystal X-ray diffraction CIFs for $Ln_2Ru_3Al_{15}$ (Ln = Ce, Gd). This material is available free of charge via the Internet at http://pubs.acs.org.

■ AUTHOR INFORMATION

Corresponding Author

*E-mail: jchan@lsu.edu.

Notes

The authors declare no competing financial interest.

■ ACKNOWLEDGMENTS

D.P.Y. acknowledges support from the National Science Foundation (NSF) through DMR1005764, E.M. acknowledges partial support from the NSF through DMR0847681, and J.Y.C. acknowledges support from the NSF through DMR1063735.

■ REFERENCES

(1) Niemann, S.; Jeitschko, W. *Z. Kristallogr.* **1995**, *210*, 338−341.
(2) Strydom, A. M. *Physica B* **2009**, *404*, 2981−2984.
(3) Nishioka, T.; Kawamura, Y.; Takesaka, T.; Kobayashi, R.; Kato, H.; Matsumura, M.; Kodama, K.; Matsubayashi, K.; Uwatoko, Y. *J. Phys. Soc. Jpn.* **2009**, *78*, 123705.
(4) Mignot, J.-M.; Robert, J.; André, G.; Bataille, A. M.; Nishioka, T.; Kobayashi, R.; Matsumura, M.; Tanida, H.; Tanaka, D.; Sera, M. *J. Phys. Soc. Jpn.* **2011**, *80*, SA022.
(5) Khalyavin, D. D.; Hillier, A. D.; Adroja, D. T.; Strydom, A. M.; Manuel, P.; Chapon, L. C.; Peratheepan, P.; Knight, K.; Deen, P.; Ritter, C.; Muro, Y.; Takabatake, T. *Phys. Rev. B* **2010**, *82*, 100405.
(6) Strigari, F.; Willers, T.; Muro, Y.; Yutani, K.; Takabatake, T.; Hu, Z.; Chin, Y. Y.; Agrestini, S.; Lin, H. J.; Chen, C. T.; Tanaka, A.; Haverkort, M. W.; Tjeng, L. H.; Severing, A. *Phys. Rev. B* **2012**, *86*, 081105.
(7) Hanzawa, K. *J. Phys. Soc. Jpn.* **2011**, *80*, 023707.
(8) Kimura, S.-i.; Iizuka, T.; Miyazaki, H.; Irizawa, A.; Muro, Y.; Takabatake, T. *Phys. Rev. Lett.* **2011**, *106*, 056404.
(9) Tanida, H.; Tanaka, D.; Sera, M.; Moriyoshi, C.; Kuroiwa, Y.; Takesaka, T.; Nishioka, T.; Kato, H.; Matsumura, M. *J. Phys. Soc. Jpn.* **2010**, *79*, 043708.
(10) Goraus, J.; Ślebarski, A. *J. Phys.: Condens. Matter* **2012**, *24*, 095503.
(11) Morrison, G.; Haldolaarachchige, N.; Young, D. P.; Chan, J. Y. *J. Phys.: Condens. Matter* **2012**, *24*, 356002.
(12) Fehrmann, B.; Jeitschko, W. *J. Alloys Compd.* **2000**, *298*, 153−159.
(13) Morrison, G. W.; Menard, M. C.; Treadwell, L. J.; Haldolaarachchige, N.; Kendrick, K. C.; Young, D. P.; Chan, J. Y. *Philos. Mag.* **2012**, *92*, 2524−2540.
(14) Tursina, A. I.; Murashova, E. V.; Nesterenko, S. N.; Chernyshev, I. V.; No, l, H.; Seropegin, Y. D. *Acta Crystallogr., Sect. E* **2004**, *60*, i145−i146.
(15) Lide, D. R. *CRC Handbook of Chemistry and Physics*, 86th ed.; Taylor & Francis: New York, 2005.
(16) Altomare, A.; Burla, M. C.; Camalli, M.; Cascarano, G.; Giacovazzo, C.; Guagliardi, A.; Moliterni, A. G. G.; Polidori, G.; Spagna, R. *J. Appl. Crystallogr.* **1999**, *32*, 115.
(17) Sheldrick, G. M. *Acta Crystallogr., Sect. A* **2008**, *64*, 112−122.
(18) Muro, Y.; Kajino, J.; Onimaru, T.; Takabatake, T. *J. Phys. Soc. Jpn.* **2011**, *80*, SA021.
(19) Emsley, J. *The Elements*, 2nd ed.; Oxford University Press: New York, 1991.
(20) Niemann, J.; Jeitschko, W. *Z. Anorg. Allg. Chem.* **2002**, *628*, 2549−2556.
(21) Murashova, E. V.; Tursina, A. I.; Bukhanko, N. G.; Nesterenko, S. N.; Kurenbaeva, Z. M.; Seropegin, Y. D.; Noël, H.; Potel, M.; Roisnel, T.; Kaczorowski, D. *Mater. Res. Bull.* **2010**, *45*, 993−999.
(22) Fujii, H.; Inoue, T.; Andoh, Y.; Takabatake, T.; Satoh, K.; Maeno, Y.; Fujita, T.; Sakurai, J.; Yamaguchi, Y. *Phys. Rev. B* **1989**, *39*, 6840−6843.
(23) Lee, W. H.; Kwan, K. S.; Klavins, P.; Shelton, R. N. *Phys. Rev. B* **1990**, *42*, 6542−6545.
(24) Williams, D. S.; Shand, P. M.; Pekarek, T. M.; Skomski, R.; Petkov, V.; Leslie-Pelecky, D. L. *Phys. Rev. B* **2003**, *68*, 214404.
(25) Ruderman, M. A.; Kittel, C. *Phys. Rev.* **1954**, *96*, 99−102.
(26) Kasuya, T. *Prog. Theor. Phys.* **1956**, *16*, 45−57.
(27) Yosida, K. *Phys. Rev.* **1957**, *106*, 893−898.
(28) Edelstein, A. S. *J. Magn. Magn. Mater.* **2003**, *256*, 430−448.
(29) Snow, C. S.; Cooper, S. L.; Young, D. P.; Fisk, Z.; Comment, A.; Ansermet, J.-P. *Phys. Rev. B* **2001**, *64*, 174412.
(30) Chan, J. Y.; Kauzlarich, S. M.; Klavins, P.; Liu, J. Z.; Shelton, R. N.; Webb, D. J. *Phys. Rev. B* **2000**, *61*, 459−463.
(31) Mazumdar, C.; Nigam, A. K.; Nagarajan, R.; Gupta, L. C.; Chandra, G.; Padalia, B. D.; Godart, C.; Vijayaraghaven, R. *J. Appl. Phys.* **1997**, *81*, 5781−5783.
(32) Takesaka, T.; Oe, K.; Kobayashi, R.; Kawamura, Y.; Nishioka, T.; Kato, H.; Matsumura, M.; Kodama, K. *J. Phys. Conf. Ser.* **2010**, *200*, 012201.